AIAA SciTech Forum
23-27 January 2023, National Harbor, MD & Online
AIAA SCITECH 2023 Forum

10.2514/6.2023-2040

Design of an Aeroelastically Scaled Model in a Compressed Air Wind Tunnel Facility Using Multifidelity Multi-Objective Bayesian Optimization

Daning Huang*, Ashwin Renganathan†, and Mark Miller‡
The Pennsylvania State University, University Park, PA, 16802

This paper presents the design of a geometrically nonlinear aeroelastically scaled model in a compressed air wind tunnel (CAWT) facility using a two-pronged approach that integrates the classical dimensional analysis and a systematic multi-disciplinary optimization procedure. The CAWT facility, recently constructed at Penn State, enables large Reynolds numbers to be tested using small models, which effectively removes the usual approximation of Reynolds number in aeroelastic wind tunnel tests. To develop the scaled model, the two-pronged approach first identifies the groups of similarity parameters of the aeroelastic model using classical dimensional analysis. Next, when some of the similarity parameters cannot be satisfied due to limitations of manufacture and test conditions, numerical optimization is performed to adjust the scaled model to maintain the similarity in the aeroelastic characteristics, such as the flutter boundary. A sample-efficient multifidelity multi-objective Bayesian optimization (M2BO) algorithm is proposed to tackle the highly nonlinear aeroelastic optimization problem. The developed methodologies are applied to the scaling of the Pazy wing model, which is designed for large deformation aeroelastic experiments. The results have demonstrated the efficacy of utilizing the CAWT facility for aeroelastic tests that enables a significantly wider range of model scales beyond that of a conventional wind tunnel, while maintaining the aerodynamic similarity. Furthermore, the two-pronged approach has been demonstrated to produce the design of a practically-viable aeroelastically scaled model in the presence of model imperfections. The initial success opens up a unique venue for the design, analysis, and testing of scaled nonlinear aeroelastic models with enhanced reproduction of operating conditions in the CAWT facility.

List of Symbols

b, c	Half-chord and full-chord lengths
c_a	Airfoil camber
$\mathbf{c}_E, \mathbf{c}_I$	Equality and inequality constraints
$c(\cdot, \cdot)$	Multifidelity cost function
$\mathcal{D}$	Observed data for Gaussian process
f_i	Model for objective i
$\mathbf{f}$	Set of models for all objectives
$\mathcal{GP}$	Gaussian process
$\mathbf{I}, I_{ij}$	Tensor of moments of inertia and its elements, $i, j = 1, 2, 3$
$\mathbf{I}_n$	Identity matrix of dimension $n \times n$
$\mathbf{K}, K_{ij}$	Effective stiffness matrix and its elements, $i, j = 1, 2, 3, 4$
$\mathbf{K}_n, \mathbf{k}_n$	Sample covariance matrix and vector in GP
k	Reduced frequency
$[L]$	Dimension of length

*Assistant Professor, Department of Aerospace Engineering, Member AIAA, daning@psu.edu
†Assistant Professor, Department of Aerospace Engineering, Member AIAA, ashwin.renganathan@psu.edu
‡Assistant Professor, Department of Aerospace Engineering, Member AIAA, mark.a.miller@psu.edu

$[M]$	Dimension of mass
m	Lumped mass
$\mathcal{P}$	Pareto front set
$\mathbf{p}, p_i$	Position vector of lumped mass and its elements, $i = 1, 2, 3$
Re	Reynolds number
$[T]$	Dimension of time
t_a	Airfoil thickness
V_∞	Freestream velocity
$\mathcal{S}$	Fidelity space
s	Model fidelity
x	Spanwise coordinate
$\mathbf{x}$	Vector of design variables
$\mathcal{X}$	Input space
y	objective observation
α_r	Root angle of attack
$\kappa_\square$	Scaling ratio for a quantity $\square$
μ	Air viscosity
μ_n	Gaussian process mean
ρ	Air density
ω	Frequency
ω_h, ω_α	Nominal bending and torsional frequency
$\mathbf{\Omega}$	Gaussian process hyperparameters
σ	Gaussian process variance
$\square_F$	Quantities at flutter point
$\square_m$	Quantities related to the scaled model
$\square_p$	Quantities related to the prototype
AePW3	The Third Aeroelastic Prediction Workshop
CAWT	Compressed Air Wind Tunnel
EHVI	Expected hypervolume improvement
GEBT	Geometrically Exact Beam Theory
M2BO	Multifidelity Multi-objective Bayesian Optimization
OOP	Out-Of-Plane
PF	Pareto frontier
SHARPy	Simulation of High Aspect Ratio airplanes and wind turbines in Python
UVLM	Unsteady Vortex Lattice Method

I. Introduction

The ever-lasting pursuit of energy efficiency in aviation has led to aircraft with increasingly flexible and light-weight structures, represented by high-aspect-ratio wing designs. Very flexible wing structures, however, are likely to undergo large nonlinear deformations during flight and experience catastrophic aeroelastic instabilities, especially flutter, of which an infamous and classical example is the Helios mishap [1].

Extensive computational efforts have been devoted to the nonlinear aeroelastic analysis of very flexible wings that account for the variation of structural modal properties and aerodynamic shape due to the geometrically nonlinear deformation [2–5]. In parallel, experimental campaigns have been developed aiming at understanding the nonlinear aeroelastic behavior and validating the computational tools. One of the early efforts is the Duke University wing test [6], which offers publicly available model and test data; however, this test model from 2001 is only marginally nonlinear

and not representative of modern flexible wing structures. A more recent experimental campaign focusing on the aeroelasticity of very flexible wing structure is the Pazy wing, developed at the Technion [7, 8], as a part of the Third Aeroelastic Prediction Workshop (AePW3) Large Deflection Group [9]. The Pazy wing serves as an excellent benchmark case that admits aeroelastic deformations up to 60% of the semispan and provides detailed model and test data for computational validation. A series of computational studies have been published for the aeroelastic modeling and flutter prediction of the Pazy wing and have achieved reasonable accuracy [10–15]. Furthermore, as a community effort, the relevant computational models have been made publicly available [13], under the open-source analysis framework of SHARPy (Simulation of High Aspect Ratio airplanes and wind turbines in Python) [16]. Such availability has enabled further experimental and computational exploration of the aeroelastic characteristics of very flexible wing structures.

The Pazy wing configuration is designed and built specifically for the nonlinear aeroelastic testing in the wind tunnel and not intended to be a scaled model for any full-size prototypes [8]. A natural question to ask after the initial success of the computational validation is: *How can the Pazy wing results inform the aeroelastic scaling, testing and analysis of a full-size very flexible wing configuration?* This question can be tackled by starting with an attempt to aeroelastically scale the Pazy wing model and identify the challenges in the scaling of such a structure with geometrically nonlinear aeroelastic deformations.

In the last seven decades, a considerable amount of research efforts have been devoted to the development of aeroelastic scaling techniques to enable the wind tunnel testing of aeroelastic problems of increasing complexity. The fundamentals of aeroelastic scaling, based on the dimensional analysis, are summarized in the classical textbook on aeroelasticity by Bisplinghoff et al. [17]. The topic of aeroelastic scaling is further expanded in the AGARD Manual on Aeroelasticity [18] with a provision of details on model construction and testing. The classical aeroelastic scaling approach has been practiced extensively at the Transonic Dynamic Tunnel at NASA Langley Research Center, which is a dedicated facility for testing aeroelastically scaled models [19]. The classical scaling methods have considered linear structures and aerodynamics, leading to the two key requirements of (1) geometrically scaling the aerodynamic shape, and (2) matching the nondimensional natural frequencies and mode shapes. Furthermore, for very flexible structures, it has been found that the linear and geometrically nonlinear components of the model follow the same scaling rule, and the nonlinear aeroelastic scaling can be achieved by matching a set of carefully selected similarity parameters, including the Froude number [20].

Nevertheless, the classical analytical scaling approach typically faces two challenges. First, the experimental configuration obtained using analytical scaling laws may require unrealistic wind tunnel conditions, materials having nonphysical properties, or prohibitive manufacturing specifications. Second, many times it is difficult to account for strong nonlinearities and coupling effects in a multidisciplinary problem, which may lead to multiple groups of similarity parameters requiring conflicting scaling laws.

The first challenge is typically addressed by redesigning the internal structure of the scaled model such that its structural dimensionless parameters are consistent with the full scale prototype. The redesign strategy for linear structures has been achieved using a modal or multidisciplinary optimization procedure [21–24]; the optimization approach has also been extended for nonlinear aeroelastic scaling problems [25, 26]. Furthermore, utilizing a wind tunnel having a capability of varying gas density and pressure can facilitate the improved matching of the similarity parameters related to aerodynamics. The second challenge has been classically addressed using the "restricted purpose" test, which ignores some coupling effects, or the "incomplete" test, which incorporates external artificial loads to compensate for the mismatch in scaling [27, 28]. Such approaches may be insufficient for modern aircraft such as those with very flexible wings, due to the strong coupling between the nonlinear structure and unsteady aerodynamics.

More recently, a systematic scaling methodology, called the two-pronged approach, was developed for the scaling of general multidisciplinary problems [29–34]. The two-pronged approach combines the classical dimensional analysis with modern numerical simulation methods, as illustrated in Fig. 1. On the left-hand branch, basic scaling requirements are established using dimensional analysis, in a manner that resembles the classical procedure. On the right-hand branch, complete multidisciplinary solutions for the prototype as well as the scaled model are obtained using numerical simulation. From the comparison and adjustment of these two models, achieved using an optimization procedure, the "numerical similarity solutions" are generated to replace the analytical similarity solutions for refinement of the scaling laws. The initial success of the two-pronged approach has been demonstrated via the aerothermoelastic scaling of high-speed aircraft structures [33, 34], where a vanilla multi-objective Bayesian optimization algorithm was employed to identify numerically scaled models from a non-convex design space to achieve simultaneous similarities in structural and thermal responses; such similarities are otherwise not achievable using classical scaling approaches.

It was found that the success of the two-pronged approach hinges on an optimization algorithm to explore the highly non-convex design space of the scaled model in a robust and efficient manner. Given the computational expense of

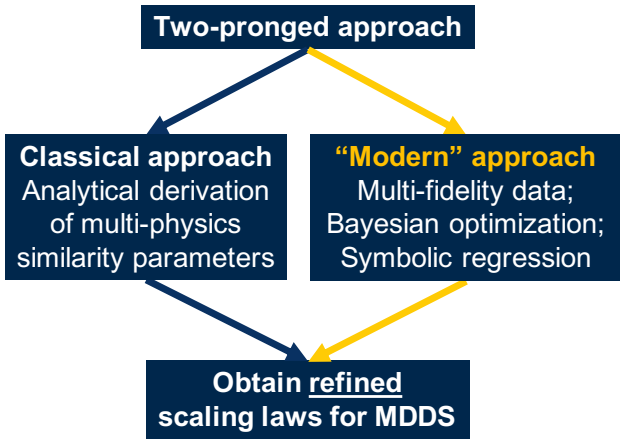

Fig. 1 Illustration of the two-pronged approach for deriving scaling laws. MDDS stands for Multi-Disciplinary Dynamical System, e.g., an aeroelastic system.

coupled nonlinear aeroelastic simulations and lack of accurate derivatives from such simulations, the two-pronged approach, previously introduced in [33, 34] can benefit from an advanced multifidelity multi-objective Bayesian optimization (M2BO) algorithm. The M2BO utilizes simulations of multiple fidelities that trade computational accuracy for efficiency. Such simulations are characterized by one or more tunable fidelity parameters (e.g., mesh resolution, linearization, etc.) which can be controlled to achieve cost-accuracy trade-off. Then, our proposed M2BO algorithm relies on learning the correlations between the models at different fidelities (see e.g., [35]) to exploit such a trade-off and result in more sample-efficient optimization. Finally, the M2BO algorithm can incorporate existing experimental data as an even higher level of fidelity information, that can be leveraged to guide the optimization process.

Recently, a new compressed air wind tunnel (CAWT) facility has been constructed at Penn State. This facility operates as a conventional single-return wind tunnel, but has an adjustable range of static pressures from atmospheric up to 34 atmospheres (500 psi). This enables large Reynolds numbers to be tested using small models as the kinematic viscosity of air is reduced upon pressurization. Key to aeroelastic scaling considerations is that only low velocities are needed to produce the correct aerodynamic similarity parameters, reducing the flow frequencies while still achieving flight-relevant conditions. This capability opens up a unique venue for the design, analysis, and testing of scaled nonlinear aeroelastic models. This paper serves as a preliminary study to design an aeroelastically scaled model for the Pazy wing configuration based on the CAWT specifications, so as to accurately reproduce its flutter characteristics. Specifically, the objectives are to

1. Formulate the classical and numerical scaling problems for the Pazy wing configuration;
2. Extend the two-pronged approach with a multifidelity multi-objective Bayesian optimization algorithm;
3. Generate aeroelastically scaled models for the Pazy wing using the two-pronged approach;
4. Explore the feasibility of performing scaled aeroelastic tests in the CAWT facility.

II. Methodology

A. Aeroelastic modeling of Pazy wing

The Pazy wing configuration is specifically designed for aeroelastic wind tunnel experiments with geometrical nonlinearity [7]. The prototype is a straight wing with a typical rib-spar structure, having span $L = 550$ mm, chord length $c = 100$ mm, and a uniform cross-section of NACA0018 with camber c_a and thickness t_a. The spar is made of Aluminum 7075 and 550 mm long, 60 mm wide, and 2.25 mm thick. A wing-tip rod is added to hold extra weights that can be used to tune the modal and flutter characteristics of the wing. The overall weight of the wing is 0.32 kg. The wing is mounted vertically, so that the gravity effect is insignificant. The images and geometrical models for the built-up wing configuration are available on the NASA AePW3 website [9].

The flutter characteristics of the Pazy wing is highly nonlinear [7, 8, 13–15]. When the wing has a nonzero root angle of attack, α_r, the wing experiences geometrically nonlinear deformation with a deformation up to 60% of the wing

span, as the freestream velocity V_∞ increases. The nonlinear deformation leads to two distinct flutter mechanisms: (1) A hump type of instability at lower velocity ($V_\infty \sim 30 - 60$ m/s) that involves the first torsion and the second out-of-plane (OOP) bending modes; and (2) regular flutter at higher velocity ($V_\infty \sim 70 - 90$ m/s) that involves the first torsion and the first (OOP) bending modes. As α_r increases, the onsets of both the hump and regular flutter behaviors occur at a lower flow velocity, while the hump instability persists for a shorter range of flow velocity.

Despite the nonlinearity of the Pazy wing problem, reasonable correlation between experimental and computational analysis has been achieved using mid-fidelity aeroelastic models that consists of nonlinear beam models and potential-flow-type aerodynamics models [8, 11, 13–15]. One of such implementations is SHARPy, that is based on the geometrically exact beam theory (GEBT) and an unsteady vortex lattice method (UVLM); the solver has been generously made open-source by the authors, together with publicly available model data for the Pazy wing [13, 16]. The SHARPy-based solution procedure starts with a nonlinear static aeroelastic trim of the wing configuration at a given α_r and V_∞, followed by a linearized stability analysis at the trim state using a reduced-order model approach. Note that while UVLM inherently assumes a potential flow formulation where the viscosity is confined to thin boundary layers and negligible, the viscous effect may be incorporated via cross-sectional corrections of the airfoil drag coefficient using Reynolds-number-dependent polar curve data, e.g., computed using XFOIL.

B. Description of CAWT

The CAWT was designed to enable high Reynolds number model testing at small physical scales. The primary component is the toroidal pressure vessel, shown as a schematic in figure 2. The vessel was manufactured to ASME standards and can withstand pressures up to 34 atm (500 psi). The vessel is filled using a Kaeser compressor system consisting of an ASD 40T rotary screw compressor followed by an N 502-G booster compressor which outputs the dried, filtered air to the CAWT vessel. To operate as a wind tunnel the CAWT requires several additional components including a 450 hp fan and drive motor combination, internal flow conditioning and test-section duct work, as well as flow guide vanes used in the four elbows. The high pressure operation of the CAWT will be enable Reynolds numbers of approximately 30 million per meter (9 million per foot) in the circular, 1.1m (42 inch) diameter test section. The highest Reynolds number condition occurs at the max anticipated velocity of 15 m/s and highest pressure, which gives a resulting flow density of approximately 40 kg/m^3. A major benefit of compressed air wind tunnels is that the dynamic viscosity of air is only weak function of pressure. An equivalent geometry water facility can only achieve an approximately fifteen times increase in Re due to the high fluid viscosity (for the same flow speed). Another key benefit of compressed air testing is the ability to vary the Reynolds number independently of the fluid velocity. This is especially useful for examining dynamic phenomena where a driving frequency is present that scales with the flow speed, such as the reduced frequency, $k = \omega V_\infty / b$. Here b is the half-chord, ω the oscillation frequency, and V_∞ the freestream velocity. In this way, we can achieve large Reynolds numbers at low flow speeds. This reduces experimental complexity and will enable a wider range of k values to be examined.

C. Formulation for aeroelastic scaling

Next, the design of an aeroelastically scaled model considering the CAWT specifications is presented, first using the classical dimensional analysis approach and then augmenting with an optimization-based numerical scaling approach. In this section, the notations $[M]$, $[L]$ and $[T]$ are employed to denote the dimensions of mass, length and time, respectively.

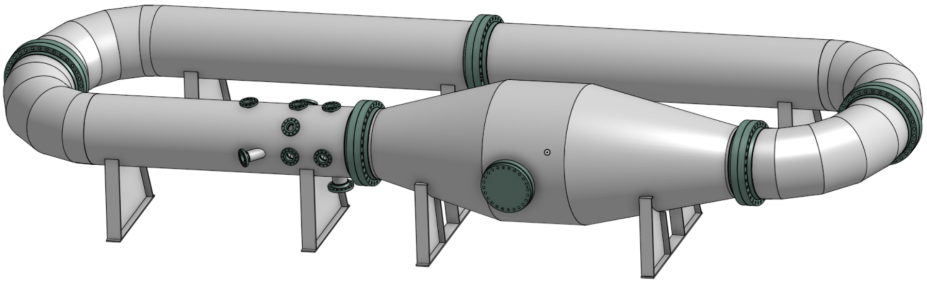

Fig. 2 Rendering of the assembled CAWT pressure vessel shell.

1. Identification of groups of similarity parameters

First, based on the mid-fidelity aeroelastic model, the key dimensional parameters governing the aeroelasticity of the Pazy wing is determined. In the UVLM model, the unsteady aerodynamic properties are completely determined by the flow conditions V and ρ, as well as the aerodynamic shape, i.e., wing span L, chord length c, airfoil camber c_a and thickness t_a. The GEBT model reduces a 3D slender structure into a 1D beam model along a reference axis, x, and the equivalent beam properties are computed at a series of stations. The inertial properties include: (1) the lumped mass $m(x)$, (2) mass offset $\mathbf{p}(x)$ as a 3×1 vector, and (3) moments of inertia $\mathbf{I}(x)$ as a symmetric 3×3 tensor. The stiffness properties are characterized by a symmetric 4×4 effective stiffness matrix $\mathbf{K}(x)$. The diagonal elements of $\mathbf{K}$, i.e., $K_{11}, K_{22}, K_{33}, K_{44}$, are associated with the stiffness factors for extension, torsion, OOP bending, and in-plane bending, respectively, while the off-diagonal terms are associated with the coupling between the four forms of deformation. Finally, the quantity of interest as the output of the aeroelastic analysis is the frequency ω of the coupled aeroelastic response.

Next, the non-dimensional similarity parameters governing the aeroelastic model are derived in two steps. In the first step, the distributions of the inertial and stiffness properties are non-dimensionalized using the quantities at the root of the wing,

$$\frac{m(\bar{x})}{m(0)}, \quad \frac{\mathbf{p}(\bar{x})}{p_1(0)}, \quad \frac{\mathbf{I}(\bar{x})}{I_{11}(0)}, \quad \frac{K_{11}(\bar{x})}{K_{11}(0)}, \quad \frac{K_{1i}(\bar{x})}{K_{12}(0)}, \quad \frac{K_{2i}(\bar{x})}{K_{22}(0)}, \quad \frac{K_{jk}(\bar{x})}{K_{33}(0)}, \ (i = 2, 3, 4; j, k = 3, 4) \tag{1}$$

where $\bar{x} = x/L$ and the dimensions of the reference quantities are, respectively, $m(0) \sim [M]$, $p_1(0) \sim [L]$ $I_{11}(0) \sim [ML^2]$, $K_{11}(0) \sim [MLT^{-2}]$, $K_{12}(0) \sim [ML^2T^{-2}]$, $K_{22}(0) \sim [ML^3T^{-2}]$, and $K_{33}(0) \sim [ML^3T^{-2}]$. Note the dimensions of $m(0)$ and $I_{11}(0)$ are due to the lumped formulation.

In the second step, introduce nominal frequencies in bending and torsion, respectively,

$$\omega_h = \sqrt{\frac{K_{33}(0)}{m(0)L^3}}, \quad \omega_\alpha = \sqrt{\frac{K_{22}(0)}{I_{11}(0)L}} \tag{2}$$

The non-dimensional similarity parameters governing the aeroelastic model, which resembles the classical set of aeroelastic similarity parameters [17, 20], are derived as

$$\text{Geometry:} \quad \frac{p_1(0)}{b}, \quad \frac{c_a}{b}, \quad \frac{t_a}{b}, \quad \frac{b}{L}; \tag{3a}$$

$$\text{Structure:} \quad \frac{m(0)}{\rho b^3}, \quad \sqrt{\frac{I_{11}(0)}{m(0)b^2}}, \quad \frac{\omega_h}{\omega_\alpha}, \quad \frac{K_{11}(0)b^2}{K_{33}(0)}, \quad \frac{K_{12}(0)b}{K_{33}(0)}; \tag{3b}$$

$$\text{Aerodynamics:} \quad Re = \frac{\rho V b}{\mu}; \tag{3c}$$

$$\text{Coupling:} \quad k = \frac{\omega b}{V}, \quad \bar{\omega} = \frac{\omega}{\omega_\alpha}. \tag{3d}$$

where by convention the half chord length $b = c/2$ is used instead of c.

Equations (1)-(3) define the complete set of similarity parameters for the Pazy wing. When compared to the classical scaling for aeroelastic flutter, an extra set of similarity parameters are introduced due to the distributed inertia and stiffness properties, as well as the stiffness coupling.

A successful aeroelastic scaling implies the reproduction of k and $\bar{\omega}$ in the scaled model, which can be achieved, theoretically, by matching the remaining groups of similarity parameters between the model and the prototype.

2. Analytical scaling using dimensional analysis

With the similarity parameters groups derived, the analytical approach is attempted to derive aeroelastically scaled models. To start with, denote the quantities associated with the model and the prototype using subscripts m and p, respectively, and introduce the notation

$$\kappa_\square = \frac{\square_m}{\square_p} \tag{4}$$

representing the scaling factor, i.e., the ratio of quantity $\square$ between the model and the prototype.

The scaling of the parameters defining the aeroelastic model boils down to the determination of the scaling factors for the fundamental quantities: length L, mass M and time T. For length, one can simply use $\kappa_L = \kappa_b$; for mass, one can use $\kappa_M = \kappa_\rho \kappa_b^3$. As for the time scaling factor, one can leverage the reduced frequency. When this quantity is matched,

$$\frac{\kappa_\omega \kappa_b}{\kappa_V} = 1 \Rightarrow \kappa_\omega = \frac{\kappa_V}{\kappa_b} \tag{5}$$

Since $\omega \sim [T^{-1}]$, the time scaling factor can be defined as $\kappa_T = \kappa_b/\kappa_V$. Observing the definitions of κ_L, κ_M and κ_T, it is clear that an aeroelastically scaled model is completely defined given κ_ρ, κ_b and κ_V.

Regular wind tunnel The Pazy wing experiment was performed in a conventional low-speed wind tunnel where the working gas is air with constant density and viscosity, i.e., $\kappa_\rho = 1$ and $\kappa_\mu = 1$. To avoid compressibility effects, the maximum flow speed in the wind tunnel needs to be lower than Mach 0.3, or approximately $V \leq 100$m/s. Since the original Pazy wing model has a flutter speed that can be as high as ~ 90m/s, the ratio $\kappa_V \leq \frac{100}{90} \approx 1.11$.

If one would like to maintain the Reynolds number similarity for the scaled model in the conventional low-speed wind tunnel,

$$\kappa_{Re} = \frac{\kappa_\rho \kappa_V \kappa_b}{\kappa_\mu} = 1 \Rightarrow \kappa_b = \kappa_V^{-1} \tag{6}$$

or $\kappa_b \geq 0.9$, i.e., it is only possible to scale the model down by a marginal 10%.

If one relaxes the Reynolds number similarity, only requiring the order of magnitude in the Reynolds number be similar, say $\kappa_{Re} \in [0.2, 1]$. Then

$$\kappa_b = \kappa_{Re} \kappa_V^{-1} \in [0.18, 0.9] \tag{7}$$

which allows for scaling down the model by a factor ~ 5.

Compressed air wind tunnel Now consider the CAWT facility, where the working gas is air with variable densities and constant viscosity. Approximately, $\kappa_\rho \in [1, 30]$ and $\kappa_\mu = 1$. The flow speed in CAWT, however, maximizes at a low value of 15m/s, which corresponds to $\kappa_V \leq \frac{15}{90} \approx 0.167$.

To maintain Reynolds number similarity in CAWT,

$$\kappa_{Re} = \frac{\kappa_\rho \kappa_V \kappa_b}{\kappa_\mu} = 1 \Rightarrow \kappa_b = (\kappa_\rho \kappa_V)^{-1} \tag{8}$$

or $\kappa_b \geq 1/5$. Therefore, unlike the conventional wind tunnel, one can obtain a scaled model in CAWT with a factor as high as 5 without sacrificing the aerodynamic similarity.

With the key scaling factors known, one may proceed to scale the rest of the parameters in the model. For example, the stiffness term, e.g., $K_{33}(0)$ scales with $[ML^3T^{-2}]$,

$$\frac{K_{33,m}(0)}{K_{33,p}(0)} = \kappa_M \kappa_b^3 \kappa_T^{-2} = \kappa_\rho \kappa_b^4 \kappa_V^2 \sim 10^{-3} \tag{9}$$

3. Numerical scaling by optimization

The CAWT facility allows for an aeroelastic scaled test with fully matched aerodynamic similarity. However, it is well known that the scaling may pose unrealistic requirements on the model construction when the structural similarity parameters are involved. For example, naively scaling the rib-spar structure by the given length scaling factor may lead to extremely thin structural members that are difficult to manufacture and maintain. A typical approach is to design the internal structure of the scaled model to match the non-dimensional distributions of equivalent inertial and stiffness properties, i.e. the similarity parameter group in Eq. (1).

Nevertheless, for the Pazy wing model, there is a disparity in the orders of magnitude of different equivalent stiffness terms: K_{11}, K_{44} and K_{14} are much larger than K_{12}, K_{23} and K_{24}. After the scaling by a factor of 10^{-3}, as shown in Eq. (9), the smaller terms, such as K_{12}, K_{23} and K_{24}, may become too small to be reproduced accurately in the manufactured model. In other words, while it is theoretically possible to obtain a perfectly aeroelastically scaled model, especially in the settings of the CAWT, the similarity parameter group in Eq. (1) might not be achievable due to manufacturing limitations, thus leading to an imperfectly scaled model.

To circumvent the practical limitations, one alternative is to use the two-pronged approach, which relaxes the scaling requirements for part of the similarity parameters, such as those for the extremely small stiffness terms. Instead of using the similarity parameters, the approach determines the relaxed stiffness terms for the scaled model via an optimization formulation, with an objective function that minimizes the differences in non-dimensional quantities of interest between the prototype and the model.

Specifically for the Pazy wing model, the goal is to match the reduced frequencies at flutter onset k_F as a function of α_r between the model and the prototype. Since there are two distinct flutter mechanisms, two functions need to be matched, which are denoted $k_{F1}(\alpha_r)$ and $k_{F2}(\alpha_r)$. For a set of selected $\{\alpha_{r,i}\}_{i=1}^{N}$, one can define two objective functions,

$$f_l = \sum_{i=1}^{N} \left| k_{Fl,m}(\mathbf{x}) - k_{Fl,p} \right|^2, \quad l = 1, 2 \tag{10}$$

where $\mathbf{x}$ is a vector of design variables consisting of the stiffness terms for the scaled model that are impractical to scale in the conventional manner, i.e., K_{12}, K_{23} and K_{24}. The function $k_{Fl,m}(\mathbf{x})$ can be evaluated using a numerical tool, such as SHARPy.

Subsequently, a multi-objective optimization problem is defined as follows,

$$\mathbf{x}^* = \arg\min_{\mathbf{x}} \mathbf{f}(\mathbf{x}) = [f_1(\mathbf{x}),\ f_2(\mathbf{x})] \tag{11a}$$

$$\text{s.t.} \quad \mathbf{c}_E(\mathbf{x}) = 0 \tag{11b}$$

$$\mathbf{c}_I(\mathbf{x}) \leq 0 \tag{11c}$$

where $\mathbf{c}_E$ are equality constraints representing the analytical scaling requirements that are still enforced, e.g., those in Eq. (3), while $\mathbf{c}_I$ are the inequality constraints representing the wind tunnel and manufacturing restrictions, e.g., requiring the stiffness terms to be larger than a threshold value.

The solution to Eq. (11) shall produce a Pareto front, i.e., a set of solutions in which one objective cannot be decreased without increasing the other objective(s). If the numerical scaling is successful, there is a particular solution in the Pareto front that achieves a balanced minimization of the two objectives, i.e., simultaneously matching the flutter characteristics in an approximate manner.

D. Multifidelity multiobjective Bayesian optimization (`M2BO`)

Our goal is to solve the multiobjective optimization problem in (11) using a multifidelity Bayesian optimization method. In this regard, we introduce a novel multifidelity multiobjective Bayesian optimization (`M2BO`) which we present as follows. Let $f_1, \ldots, f_m$ denote the m objectives which are unknown but observable functions defined as $f_i : \mathcal{X} \to \mathbb{R}$, where $\mathcal{X} \subset \mathbb{R}^d$ is a compact domain. Note that we will present a generalized formulation here, but for our actual application $m = 2$ and the J's are some affine functions of f. Furthermore, we assume that we have lower fidelity approximations for each model available, of the form $\hat{f}_1, \ldots, \hat{f}_m$, where $\hat{f}_i : \mathcal{X} \times \mathcal{S} \to \mathbb{R}$ with $\mathcal{S}$ being the fidelity domain. That is $\forall \mathbf{x} \in \mathcal{X}$, $s \in \mathcal{S}$, $\hat{f}_i(\mathbf{x}, s)$ corresponds to an approximation to the function f_i at fidelity s. Note that we assume, without loss of generality, that $\mathcal{S} = [0, 1]$, where $\hat{f}_i(\mathbf{x}, 1) := f_i(x)$ and thus lower values of s corresponds to lower fidelities. We also assume there is a known *cost function* $c(\mathbf{x}, s) : \mathcal{X} \times \mathcal{S} \to \mathbb{R}_+$ which quantifies the cost of querying each model at some input-fidelity pair $(\mathbf{x}, s)$.

Our approach is to place a Gaussian process (GP) prior on each model as follows:

$$\begin{aligned} \hat{f}_1 &\sim \mathcal{GP}(0, k_1(\cdot, \cdot)) \\ &\vdots \\ \hat{f}_m &\sim \mathcal{GP}(0, k_m(\cdot, \cdot)), \end{aligned} \tag{12}$$

where we have assumed that each GP has zero-mean and a positive definite kernel function $k_i : (\mathcal{X} \times \mathcal{S}) \times (\mathcal{X} \times \mathcal{S}) \to \mathbb{R}$. In this work, we assume that each GP is independent of the others and are initially constructed with a set of *seed*

observations as follows:

$$\begin{aligned} y_{1,j} &= \hat{f}_1(\mathbf{x}_j, s_j) + \epsilon_1; \quad \mathcal{D}_{1,n} = \{(\mathbf{x}_j, s_j), \hat{f}_1(\mathbf{x}_j, s_j)\}_{j=1}^n \\ &\vdots \\ y_{m,j} &= \hat{f}_m(\mathbf{x}_j, s_j) + \epsilon_m; \quad \mathcal{D}_{m,n} = \{(\mathbf{x}_j, s_j), \hat{f}_m(\mathbf{x}_j, s_j)\}_{j=1}^n, \end{aligned} \tag{13}$$

where $\mathcal{D}_{i,n},\ i = 1, \ldots, m$ is the set of observations for the ith objective, and $\epsilon_i \sim \mathcal{N}(0, \sigma^2_{\epsilon,i})$ are Gaussian white noise with unknown variance $\sigma^2_{\epsilon,i}$. Due to the independence of GPs and by virtue of a Gaussian likelihood that we assume, the posterior distributions of our GPs, conditioned on the observations are derived via Bayes' law and given by [36]

$$\begin{aligned} \hat{f}_i(\mathbf{x}, s) | \mathcal{D}_{i,n}, \mathbf{\Omega}_i &\sim \mathcal{GP}(\mu_{n,i}(\mathbf{x}, s), \sigma^2_{n,i}(\mathbf{x}, s)), \\ \mu_{n,i}(\mathbf{x}, s) &= \mathbf{k}_{n,i}^\top [\mathbf{K}_{n,i} + \sigma^2_{\epsilon,i} \mathbf{I}_n]^{-1} \mathbf{y}_n \\ \sigma^2_{n,i}(\mathbf{x}, s) &= k((\mathbf{x}, s), (\mathbf{x}, s)) - \mathbf{k}_{n,i}^\top [\mathbf{K}_{n,i} + \sigma^2_{\epsilon,i} \mathbf{I}_n]^{-1} \mathbf{k}_{n,i}, \end{aligned} \tag{14}$$

where $\mathbf{k}_{n,i}$ is a vector of covariances between $(\mathbf{x}, s)$ and all observed points in $\mathcal{D}_{i,n}$, $\mathbf{K}_n$ is a sample covariance matrix of observed points in $\mathcal{D}_{i,n}$, $\mathbf{I}_n$ is the identity matrix, and $\mathbf{y}_{i,n}$ is the vector of all observations in $\mathcal{D}_{i,n}$; (14) is then used as a surrogate model for `M2BO`. The hyperparameters $\mathbf{\Omega}_i$ are estimated by maximizing the marginal log likelihood of each GP. Note that $\mu_{n,i}$ and $\sigma^2_{n,i}$ are the posterior mean and variance of the GP, respectively, where the subscript n implies the conditioning based on n past observations.

We are interested in identifying a *Pareto optimal* set $\mathcal{P}^*$ of our objectives. We say that $\mathbf{f} = \{f_1, \ldots, f_m\}$ *dominates* another solution $\mathbf{f} \succ \mathbf{f}'$ if $f_i(\mathbf{x}, s) \geq f_i(\mathbf{x}', s'),\ \forall i \in [m]$ and $\exists\ i \in [m]$ for which $f_i(\mathbf{x}, s) > f_i(\mathbf{x}', s')$. The *Pareto frontier* (PF) is defined as $\mathcal{P}^* = \{\mathbf{f}(\mathbf{x}) : \mathbf{x} \in \mathcal{X} \nexists\ \mathbf{x}' \in \mathcal{X} : \mathbf{f}(\mathbf{x}') \succ \mathbf{f}(\mathbf{x})\}$. A measure of the quality of the PF is the hypervolume (HV) of the region of the objective space that is dominated by PF and bounded from below by a reference point.

Our goal is to estimate the PF in a sequential fashion by seeking to expand the hypervolume. We achieve this via our proposed `M2BO` approach, where we introduce a multifidelity expected hypervolume improvement (EHVI) acquisition function. Existing works that use the EHVI approach [37–41] do not acount for the fact that we could have multiple fidelities for each objective function, and thus that becomes our main focus.

1. Single fidelity multi-objective Bayesian optimization

We begin by providing an overview of multi-objective Bayesian optimization with just one fidelity level (high fidelity). Then, we will show the extensions to the proposed `M2BO`. As previously mentioned, in the multi-objective BO, we are interested in optimizing a set of objectives $\{f_1, \ldots, f_m\}$, using m independent GP models fit from data. Let the reference point be denoted $\mathbf{x}_{\text{ref}}$ which represents the ideal $\mathbf{x}$, then the hypervolum is defined as the m dimensional volume of a hypercube in the output space bounded by $\mathbf{x}_{\text{ref}}$ on one side and $\mathcal{P}^*$ on the other. Therefore, akin to [42], we can define the HV improvement (HVI) due to a candidate point $\mathbf{x}$ as

$$HVI(\mathbf{x}) = HV\left(\mathcal{P} \bigcup \{\mathbf{x}, y\}; \mathbf{x}_{\text{ref}}\right) - HV(\mathcal{P}; \mathbf{x}_{\text{ref}}). \tag{15}$$

In (15), we essentially are quantifying the improvement in the HV estimate due to a candidate point $\mathbf{x}$ and its observation y. If $\mathcal{P}$ already dominates y then, naturally, $HVI = 0$. In practice, we hypothesize y with a draw from the joint posterior GP over all the m outputs and take the expectation to define the expected hypervolume improvement (EHVI) acquisition function [37, 43] defined as

$$EHVI(\mathbf{x}) = \mathbb{E}_Y\left[HV\left(\mathcal{P} \bigcup \{\mathbf{x}, Y\}; \mathbf{x}_{\text{ref}}\right) - HV(\mathcal{P}; \mathbf{x}_{\text{ref}})\right]. \tag{16}$$

We use the box decomposition method proposed by Yang et al. [44] to compute the hypervolume. The acquisition function (and its gradient) are estimated via Monte Carlo (MC) sampling from the joint posterior GP and taking sample averages. Using a fixed set of base samples, we use the quasi MC approach to evaluate and optimize a stochastic approximation of the acquisition function in (16).

Algorithm 1: Multifidelity multi-objective Bayesian optimization (`M2BO`)

Given: $\mathcal{D}_n = \{(\mathbf{x}_i, s_i), (\hat{y}_i, \ldots, \hat{y}_m)\}_{i=1}^n$, total number of rounds q, cost model $c(\cdot)$, reference point $[\mathbf{x}_{\text{ref}}, s_{\text{ref}}]$ and GP hyperparameters $\mathbf{\Omega}$

Result: Pareto front $\mathcal{P}$

for $i = n+1, \ldots, q,$ **do**

  Find $\mathbf{x}_i, s_i \in \underset{(\mathbf{x},s)\in\mathcal{X}\times\mathcal{S}}{arg\,max}\ MFEHVI(\mathbf{x}, s)$ (acquisition function maximization)

  Observe $\hat{y}_{j,i} = \hat{f}_j(\mathbf{x}_i, s_i),\ j = 1, \ldots, m$

  Evaluate cost $c_i = c(s_i)$

  Append $\mathcal{D}_{j,i} = \mathcal{D}_{j,i-1} \cup \{(\mathbf{x}_i, s_i), \hat{y}_{j,i}\}$

  Update GP hyperparameters $\mathbf{\Omega}$

Pareto front estimation:

  Sample a dense set $X_{\text{test}} \in \mathcal{X} \times \{1\}$, where $|X_{\text{test}}| = M$ and X_{test} is only at the highest fidelity $s = 1$. We typically set $M = 10^5$.

  Evaluate GP posterior means $\mu_{q,j}(X_{\text{test}}),\ \forall j = 1, \ldots, m$.

  Identify non dominated points $ndind = \texttt{isnondominated}(\{\mu_{q,1}, \ldots, \mu_{q,m}\})$.

  $\mathcal{P} = X_{\text{test}}[ndinds]$

2. Multifidelity multi-objective Bayesian optimization

For the `M2BO`, we use the "fidelity objective augmented" approach proposed by Irshad et al. [45]. The main idea is that we add an $(m+1)$th objective as a monotonically increasing function of s, that is $f_{m+1} := f_{m+1}(s)$. The reason behind requiring f_{m+1} to be monotonic (increasing) is that as we maximize the m objectives, the $m+1$th objective, if monotonic, will drive the acquisitions closer to $s = 1$. As with several existing multifidelity approaches [46–48], the acquisition function can be penalized by a cost function $c(s) : \mathcal{S} \to \mathbb{R}_+$ to penalize too much exploitation of $s = 1$ (highest fidelity and most expensive model).

Let $\mathcal{P}_s$ be the Pareto set obtained over the $m+1$ objectives $[\mathbf{f}, f_s]$ and $[\mathbf{x}_{\text{ref}}, s_{\text{ref}}]$ be the reference point in the augmented input-fidelity space. Then, our multifidelity acquisition function, $MFEHVI$, is defined as

$$MFEHVI(\mathbf{x}, s) = \frac{\mathbb{E}_Y\left[HV\left(\mathcal{P}_{s=1} \bigcup \{(\mathbf{x}, s), Y\}; [\mathbf{x}_{\text{ref}}, s_{\text{ref}}]\right) - HV(\mathcal{P}_{s=1}; [\mathbf{x}_{\text{ref}}, s_{\text{ref}}])\right]}{c(s)} \tag{17}$$

The overall algorithm is summarized in Algorithm 1 and we provide a simple synthetic example to illustrate the method as follows. We consider the multifidelity Branin-Currin function introduced in [45] and presented here below.

$$\begin{aligned} f_1(\mathbf{x}, s) &= -\left[a_1(x_{22} - a_2(s)x_{11}^2 + a_3(s)x_{11} - r)^2 + p(1 - t(s))\cos(x_{11}) + p\right] \\ f_2(\mathbf{x}, s) &= -\left[(1 - 0.1(1-s)\exp(-1/2x_2))\,\frac{2300x_1^3 + 1900x_1^2 + 2092x_1 + 60}{100x_1^3 + 500x_1^2 + 4x_1 + 20}\right], \end{aligned} \tag{18}$$

where $x_{11} = 15x_1 - 5$, $x_{22} = 15x_2$, $a_1 = 1, a_2(s) = 5.1/(4\pi^2) - 0.01(1-s)$, $a_3(s) = 5/\pi - 0.1(1-s)$, $r = 6,\ p = 10,\ t(s) = 1/8\pi + 0.05(1-s)$. We scale the inputs and outputs such that $\mathcal{X}\times\mathcal{S} = [0,1]^{d+1}$ and $y_i \in [0,1], \forall i = 1, \ldots, m$.

The Pareto front, predicted at the highest fidelity $s = 1$, and the % HV (with respect to true HV) predicted at the highest fidelity are shown in Figure 3. Note that the true HV is an estimate from 10000 MC samples from $\mathcal{X} \times \{a\}$ and evaluating the true functions f_1 and f_2 at these points.

In Figure 4, we compare the proposed multifidelity approach against the single fidelity approach where s is defaulted to 1. Here, we use a cost function $c(s) = \exp(5s)$ for both approaches and start each of them with a set of $n = 15$ seed points. Note that whereas for the multifidelity approach, the 15 seed points were uniformly and randomly distributed across the fidelity space, the single fidelity approach had all 15 points at $s = 1$. Therefore, in a way, the single fidelity is provided with more *information* than the multifidelity approach at the begining of the algorithm. Then, we repeat each experiment a total of 3 times where each time the seed samples are randomly chosen; in Figure 4 we show all 3 repetitions. Finally, both approaches were run for a total of 45 iterations. Notice that the multifidelity approach converges closer to the true HV in less than 1/3 of the cost it takes for the single fidelity approach.

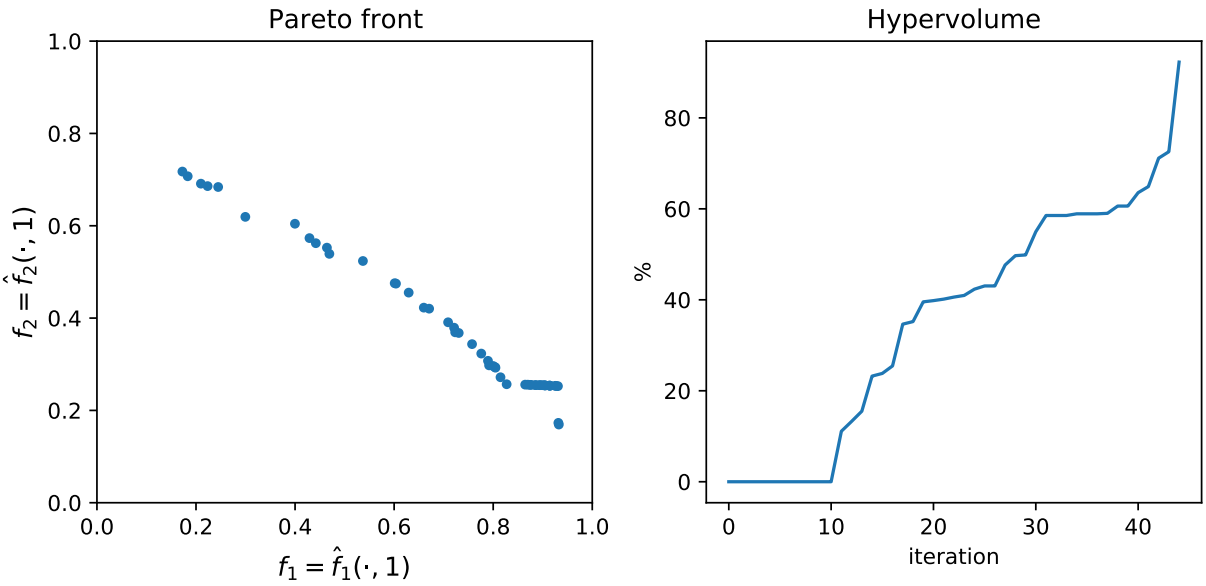

Fig. 3 Demonstration of `M2BO` on the multifidelity Branin-Currin function. Left: Pareto front, right: % true hypervolume predicted; true hypervolume is estimated from a dense MC sample set of size 10000.

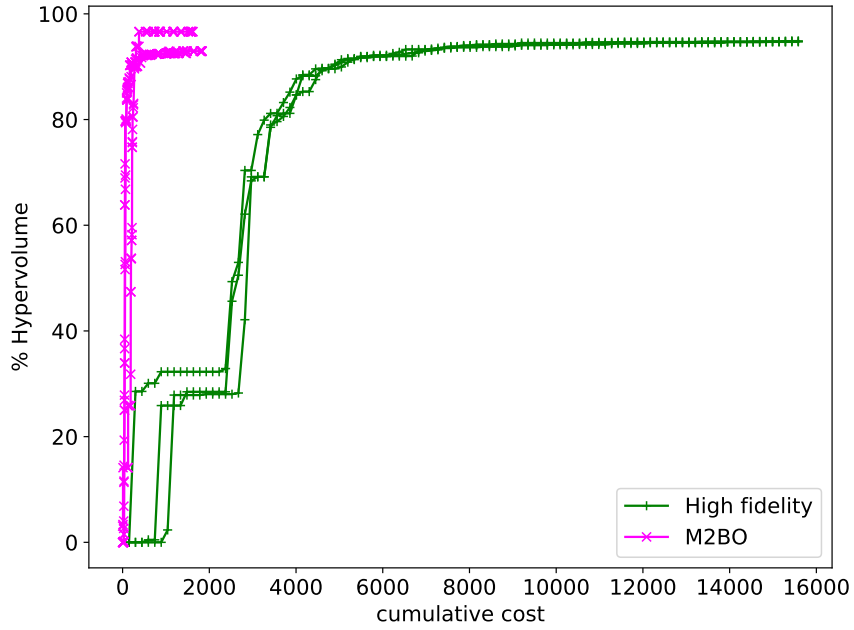

Fig. 4 Comparison of the `M2BO` against the multi-objective BO having high fidelity information.

III. Results and Discussion

In this section, we present the results for aeroelastically scaled models, first based on the analytical method, and then using the optimization-based approach.

A. Analytically scaled aeroelastic models

Two aeroelastically scaled models, Model 1 and Model 2, based on analytical scaling relations are considered. Their main similarity parameters are scaled in the same manner, as shown in Table 1. The difference is that, in Model 1, all the nondimensional equivalent beam properties in Eq. (1) are matched with those of the prototype, while in Model 2, only part of the beam properties are matched to emulate the limitations in manufacturing. Specifically, the non-matching properties of Model 2 include: $K_{12} = K_{13} = 0$ and $K_{ij} = 0$ for $i, j = 2, 3, 4$ but $i \neq j$.

To demonstrate the impact of imperfect aeroelastic scaling, the modal and flutter characteristics of the two models are compared against the prototype. In Fig. 5, the first three natural frequencies of the models are compared as a function of the freestream velocity at $\alpha_r = 7$deg, in which case the wing experiences a deformation larger than 30% of the span. Note that the frequencies vary with flow speed due to the increase in the static aeroelastic deformation. The frequencies of Model 1 matches with those of the prototype almost perfectly, indicating that the aeroelastic scaling works for both the geometrically nonlinear deformation and the modal properties. For Model 2, as expected, the predicted natural frequencies are not as accurate as those in Model 1, due to the mismatch in stiffness distributions. Still considering the case of $\alpha_r = 7$deg, in Fig. 6, the damping ratio curves of the models showing the hump mode are compared with the prototype. Model 1 exactly reproduces not only the flutter point, but also the entire flutter characteristics over the range of flow speed considered. For Model 2, there is a mode switching behavior due to the numerical eigenvalue solver, and aside from that, the flutter point is shifted by 3%.

Quantity	Scaling factor	Value
All lengths	κ_b	0.5
V	κ_V	0.1667
ρ	κ_ρ	12
$m(0)$	$\kappa_\rho \kappa_b^3$	1.5
$I_{11}(0)$	$\kappa_\rho \kappa_b^5$	0.375
$K_{11}(0)$	$\kappa_\rho \kappa_b^2 \kappa_V^2$	8.333×10^{-2}
$K_{12}(0)$	$\kappa_\rho \kappa_b^3 \kappa_V^2$	4.167×10^{-2}
$K_{22}(0), K_{33}(0)$	$\kappa_\rho \kappa_b^4 \kappa_V^2$	2.083×10^{-3}

Table 1 Aeroelastic scaling factors for Models 1 and 2.

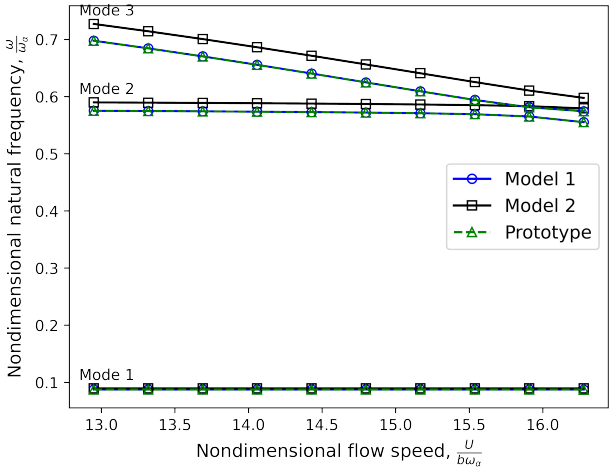

Fig. 5 The natural frequencies for the prototype and the scaled models at $\alpha_r = 7$deg.

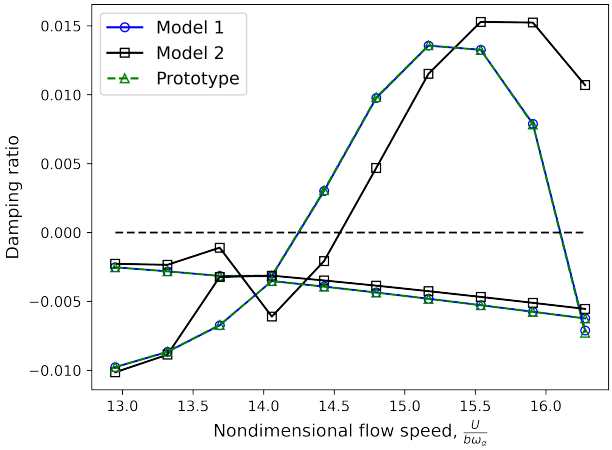

Fig. 6 The damping ratios for the prototype and the scaled models at $\alpha_r = 7$deg.

B. Optimally scaled aeroelastic models

Next, the nonzero stiffness properties of Model 2 are optimized to produce modal and flutter characteristics that can more authentically reproduce those of the prototype. Specifically, the `M2BO` algorithm is used to minimize the errors in the reduced frequencies at the onset and the exit of the hump mode; the logarithms of the errors are used as the objective functions, denoted f_1 and f_2. Solvers of two levels of fidelity ($s = \{0, 1\}$) are constructed by choosing different model discretization parameters.

The Pareto front associated with the aeroelastic scaling is shown in Fig. 7, with contours of the average $(f_1 + f_2)/2$. It indicates the trade-off of the errors in the onset and the exit of the hump mode. The solutions near "Biased 1" show the case where the exit frequencies of the model and the prototype almost match exactly at the price of erroneous onset frequency in the model. Similarly, the solutions near "Biased 2" indicate the opposite trend. On the contrary, the solutions near "Balanced" achieve a balance between the errors in both the onset and the exit frequencies, which represent a good numerically scaled aeroelastic model. In addition, note that the Pareto front is concave. This means that if one solves the numerical scaling problem with a single-objective formulation, e.g., with the averaged objective $(f_1 + f_2)/2$, then it is impossible to identify the balanced solutions such as Example 2.

The aeroelastic solutions associated with the labelled example solutions are compared with the prototype and the incorrectly-scaled Model 2 from the previous section, as shown in Fig. 8. Clearly, "Biased 1" and "Biased 2" reproduce the exit and onset frequencies, respectively, but fail to capture the other frequency. "Balanced" achieves a balanced match in both the onset and exit frequencies. This marks the initial success of the numerical scaling of a nonlinear aeroelastic model.

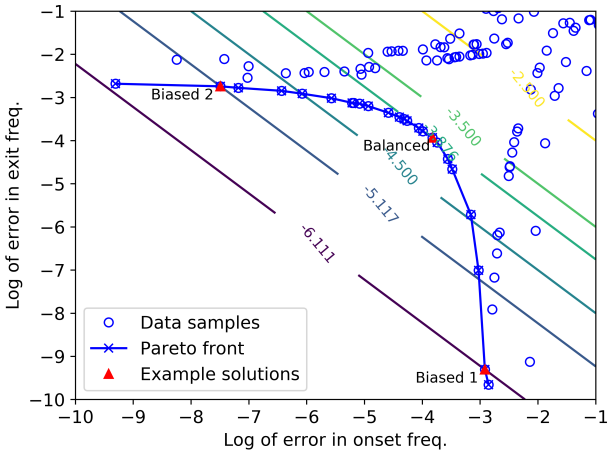

Fig. 7 The Pareto front of the aeroelastic scaling problem.

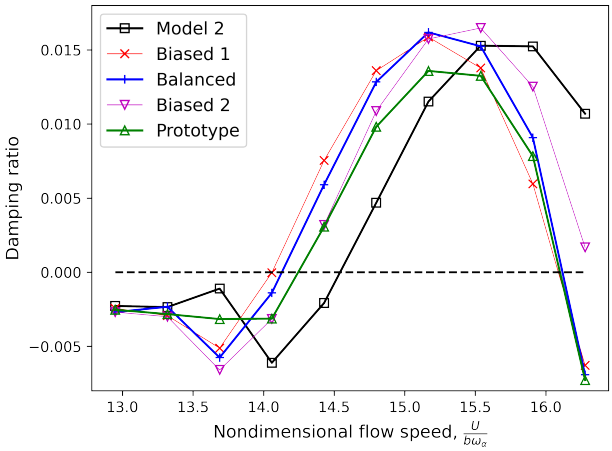

Fig. 8 The damping ratios for the prototype and different optimization-based scaled models at $\alpha_r = 7$deg.

IV. Concluding Remarks

This study presents a preliminary study on the design of an aeroelastic scaled model for a wing configuration with large geometrically nonlinear deformation in the context of a compressed air wind tunnel (CAWT) facility. A complete set of similarity parameters for the aeroelastic model has been identified using the classical dimensional analysis approach. It is demonstrated that, by leveraging the unique capabilities of CAWT, the wing configuration can be scaled perfectly by matching all the structural and aerodynamic similarity parameters, including the Reynolds number. However, the scaling of a model may pose unrealistic requirements on manufacturing, leading to an imperfectly scaled model that may produce inaccurate flutter characteristics. The design of a practically-viable aeroelastically scaled model is posed as an optimization problem, following the formulation of the so-called two-pronged approach. The optimization problem enforces a partial set of similarity parameters and imposes constraints on design variables representing the limitations in, e.g., manufacture and test conditions.

The optimization problem is solved using a multifidelity multi-objective Bayesian optimization (M2BO) algorithm, which leverages numerical solvers of multiple fidelities to achieve and exploit a cost-accuracy trade-off to result in more sample-efficient optimization. The optimized "numerically-scaled" model is benchmarked against the scaled models obtained using classical scaling approach and is demonstrated to accurately reproduce the modal and flutter characteristics of the wing configuration. The optimization-based numerical scaling approach opens up a unique venue for the design, analysis, and testing of scaled nonlinear aeroelastic models with enhanced reproduction of operating

conditions using the CAWT facility.

References

[1] Noll, T. E., Brown, J. M., Perez-Davis, M. E., Ishmael, S. D., Tiffany, G. C., and Gaier, M., "Investigation of the Helios Prototype Aircraft Mishap Volume I Mishap Report," *NASA Report*, Vol. 9, 2004.

[2] Su, W., and Cesnik, C. E., "Dynamic Response of Highly Flexible Flying Wings," *AIAA Journal*, Vol. 49, No. 2, 2011, pp. 324–339.

[3] Ritter, M., Cesnik, C. E., and Krüger, W. R., "An Enhanced Modal Approach for Large Deformation Modeling of Wing-like Structures," *56th AIAA/ASCE/AHS/ASC Structures, Structural Dynamics, and Materials Conference*, 2015, pp. 1–16.

[4] Kantor, E., Raveh, D. E., and Cavallaro, R., "Nonlinear Structural, Nonlinear Aerodynamic Model for Static Aeroelastic Problems," *AIAA Journal*, Vol. 57, No. 5, 2019, pp. 2158–2170.

[5] Jonsson, E., Riso, C., Lupp, C. A., Cesnik, C. E., Martins, J. R., and Epureanu, B. I., "Flutter and Post-flutter Constraints in Aircraft Design Optimization," *Progress in Aerospace Sciences*, Vol. 109, 2019, p. 100537.

[6] Tang, D., and Dowell, E. H., "Experimental and Theoretical Study on Aeroelastic Response of High-aspect-ratio Wings," *AIAA Journal*, Vol. 39, No. 8, 2001, pp. 1430–1441.

[7] Avin, O., Raveh, D. E., Drachinsky, A., Ben-Shmuel, Y., and Tur, M., "An Experimental Benchmark of a Very Flexible Wing," *AIAA SciTech 2021 Forum*, 2021, pp. 1–32.

[8] Avin, O., Raveh, D. E., Drachinsky, A., Ben-Shmuel, Y., and Tur, M., "Experimental Aeroelastic Benchmark of a Very Flexible Wing," *AIAA Journal*, Vol. 60, No. 3, 2022, pp. 1745–1768.

[9] Large Deflection Working Group, "NASA Aeroelastic Prediction Workshop," `https://nescacademy.nasa.gov/workshops/AePW3/public/wg/largedeflection`, 2022. [Online; accessed 01-June-2022].

[10] Riso, C., and Cesnik, C. E., "Correlations Between UM/NAST Nonlinear Aeroelastic Simulations and the Pre-Pazy Wing Experiment," *AIAA Scitech 2021 Forum*, 2021, pp. 1–24. doi:10.2514/6.2021-1712.

[11] Riso, C., and Cesnik, C. E., "Low-Order Geometrically Nonlinear Aeroelastic Modeling and Analysis of the Pazy Wing Experiment," *AIAA SCITECH 2022 Forum*, 2022, pp. 1–30. doi:10.2514/6.2022-2313.

[12] Goizueta, N., Wynn, A., and Palacios, R., "Fast Flutter Evaluation of Very Flexible Wing Using Interpolation on an Optimal Training Dataset," *AIAA SCITECH 2022 Forum*, 2022, pp. 1–21. doi:10.2514/6.2022-1345.

[13] Goizueta, N., Wynn, A., Palacios, R., Drachinsky, A., and Raveh, D. E., "Flutter Predictions for Very Flexible Wing Wind Tunnel Test," *Journal of Aircraft*, 2022, pp. 1–16.

[14] Hilger, J., and Ritter, M. R., "Nonlinear Aeroelastic Simulations and Stability Analysis of the Pazy Wing Aeroelastic Benchmark," *Aerospace*, Vol. 8, No. 10, 2021, p. 308.

[15] Righi, M., Carnevali, L., and Ravasi, M., "Uncertainties Quantification in Flutter Prediction of a Wind Tunnel Model Exhibiting Large Displacements," *AIAA SCITECH 2022 Forum*, 2022, pp. 1–10. doi:10.2514/6.2022-0178.

[16] del Carre, A., Muñoz-Simón, A., Goizueta, N., and Palacios, R., "SHARPy: A dynamic aeroelastic simulation toolbox for very flexible aircraft and wind turbines," *Journal of Open Source Software*, Vol. 4, No. 44, 2019, p. 1885.

[17] Bisplinghoff, R. L., Ashley, H., and Halfman, R. L., *Aeroelasticity*, Addison-Wesley Publishing Company, 1955.

[18] Wasserman, L. S., and Mykytow, W. J., "Model Construction, Part IV," *AGARD Manual on Aeroelasticity*, Vol. 7, 1963, pp. 1–30.

[19] Ivanco, T. G., "Unique Testing Capabilities of the NASA Langley Transonic Dynamics Tunnel, an Exercise in Aeroelastic Scaling," *AIAA 2013-2625, Ground Testing Conference*, 2013, pp. 1–23.

[20] Wan, Z., and Cesnik, C. E., "Geometrically Nonlinear Aeroelastic Scaling for Very Flexible Aircraft," *AIAA Journal*, Vol. 52, No. 10, 2014, pp. 2251–2260.

[21] French, M., "An Application of Structural Optimization in Wind Tunnel Model Design," *AIAA-90-0956-CP, 31st Structures, Structural Dynamics and Materials Conference*, Long Beach, CA, 1990, pp. 127–134.

[22] French, M., and Eastep, F., "Aeroelastic Model Design Using Parameter Identification," *Journal of Aircraft*, Vol. 33, No. 1, 1996, pp. 198–202.

[23] Richards, J., Suleman, A., Canfield, R., and Blair, M., "Design of a Scaled RPV for Investigation of Gust Response of Joined-Wing Sensorcraft," *50th AIAA/ASME/ASCE/AHS/ASC Structures, Structural Dynamics, and Materials Conference 17th AIAA/ASME/AHS Adaptive Structures Conference 11th AIAA No*, Palm Springs, CA, 2009, pp. 1–14. doi:10.2514/2009-2218.

[24] Mas-Colomer, J., "Aeroelastic Similarity of a Flight Demonstrator via Multidisciplinary Optimization," Ph.D. thesis, Universite de Toulouse, Toulouse, French, 2018.

[25] Bond, V. L., Canfield, R. A., Suleman, A., and Blair, M., "Aeroelastic Scaling of a Joined Wing for Nonlinear Geometric Stiffness," *AIAA Journal*, Vol. 50, No. 3, 2012, pp. 513–522.

[26] Ricciardi, A. P., "Geometrically Nonlinear Aeroelastic Scaling," Ph.D. thesis, Virginia Tech, Blacksburg, Virginia, 2014.

[27] Calligeros, J. M., and Dugundji, J., "Similarity Laws Required for Experimental Aerothermoelastic Studies. Part 2 Hypersonic Speeds," Tech. Rep. TR 75–2, Office of Naval Research, 1961.

[28] Dugundji, J., and Calligeros, J. M., "Similarity Laws for Aerothermoelastic Testing," *Journal of the Aerospace Sciences*, Vol. 29, No. 8, 1962, pp. 935–950. doi:10.2514/8.9663.

[29] Friedmann, P., Guillot, D., and Presente, E., "Adaptive Control of Aeroelastic Instabilities in Transonic Flow and Its Scaling," *Journal of Guidance, Control, and Dynamics*, Vol. 20, No. 6, 1997, pp. 1190–1199.

[30] Friedmann, P. P., "Innovative Scaling Laws for Study of Nonlinear Aeroelastic and Aeroservoelastic Problems." Tech. Rep. AFRL-SR-BL-TR-98-0564, Univ. of California, Dept. of Mechanical and Aerospace Engineering, Los Angeles, CA, Apr. 1998.

[31] Friedmann, P., and Presente, E., "Active Control of Flutter in Compressible Flow and Its Aeroelastic Scaling," *Journal of Guidance, Control, and Dynamics*, Vol. 24, No. 1, 2001, pp. 167–175.

[32] Friedmann, P., "Aeroelastic Scaling for Rotary-Wing Aircraft With Applications," *Journal of Fluids and Structures*, Vol. 19, No. 5, 2004, pp. 635–650. doi:10.1016/j.jfluidstructs.2004.03.003.

[33] Daning Huang, "Development of a Hypersonic Aerothermoelastic Framework and Its Application to Flutter and Aerothermoelastic Scaling of Skin Panels," Ph.D. thesis, University of Michigan, Ann Arbor, MI, 2019.

[34] Huang, D., Friedmann, P. P., and Rokita, T., "Aerothermoelastic Scaling Laws for Hypersonic Skin Panel Configurations with Arbitrary Flow Orientation," *AIAA Journal*, 2019, pp. 1–16. doi:10.2514/1.J057499.

[35] Renganathan, S. A., Rao, V., and Navon, I. M., "CAMERA: A Method for Cost-aware, Adaptive, Multifidelity, Efficient Reliability Analysis," *arXiv preprint arXiv:2203.01436*, 2022.

[36] Rasmussen, C. E., and Williams, C. K. I., *Gaussian Processes for Machine Learning*, MIT Press, 2006. doi:10.7551/mitpress/3206.001.0001.

[37] Emmerich, M. T., Giannakoglou, K. C., and Naujoks, B., "Single-and multiobjective evolutionary optimization assisted by Gaussian random field metamodels," *IEEE Transactions on Evolutionary Computation*, Vol. 10, No. 4, 2006, pp. 421–439.

[38] Daulton, S., Balandat, M., and Bakshy, E., "Differentiable expected hypervolume improvement for parallel multi-objective Bayesian optimization," *Advances in Neural Information Processing Systems*, Vol. 33, 2020, pp. 9851–9864.

[39] Knowles, J., "ParEGO: A hybrid algorithm with on-line landscape approximation for expensive multiobjective optimization problems," *IEEE Transactions on Evolutionary Computation*, Vol. 10, No. 1, 2006, pp. 50–66.

[40] Konakovic Lukovic, M., Tian, Y., and Matusik, W., "Diversity-guided multi-objective bayesian optimization with batch evaluations," *Advances in Neural Information Processing Systems*, Vol. 33, 2020, pp. 17708–17720.

[41] Bradford, E., Schweidtmann, A. M., and Lapkin, A., "Efficient multiobjective optimization employing Gaussian processes, spectral sampling and a genetic algorithm," *Journal of global optimization*, Vol. 71, No. 2, 2018, pp. 407–438.

[42] Jones, D. R., Schonlau, M., and Welch, W. J., "Efficient global optimization of expensive black-box functions," *Journal of Global optimization*, Vol. 13, No. 4, 1998, pp. 455–492.

[43] Yang, K., Emmerich, M., Deutz, A., and Bäck, T., "Multi-objective Bayesian global optimization using expected hypervolume improvement gradient," *Swarm and evolutionary computation*, Vol. 44, 2019, pp. 945–956.

[44] Yang, K., Emmerich, M., Deutz, A., and Bäck, T., "Efficient computation of expected hypervolume improvement using box decomposition algorithms," *Journal of Global Optimization*, Vol. 75, No. 1, 2019, pp. 3–34.

[45] Irshad, F., Karsch, S., and Döpp, A., "Expected hypervolume improvement for simultaneous multi-objective and multi-fidelity optimization," *arXiv preprint arXiv:2112.13901*, 2021.

[46] Renganathan, S. A., Rao, V., and Navon, I. M., "CAMERA: A method for cost-aware, adaptive, multifidelity, efficient reliability analysis," *Journal of Computational Physics*, Vol. 472, 2023, p. 111698.

[47] Renganathan, S. A., Larson, J., and Wild, S., "Recursive two-step lookahead expected payoff for time-dependent bayesian optimization," *arXiv preprint arXiv:2006.08037*, 2020.

[48] Renganathan, S. A., Larson, J., and Wild, S. M., "Lookahead acquisition functions for finite-horizon time-dependent bayesian optimization and application to quantum optimal control," *arXiv preprint arXiv:2105.09824*, 2021.